COMMUNICATION SCIENCES INSTITUTE

Design and implementation of novel optical subsystems for enhancing spectral efficiency, security, and performance of high-speed WDM and OCDMA links

by

Paniz Ebrahimi

CSI-04-12-01

USC VITERBI SCHOOL OF ENGINEERING
UNIVERSITY OF SOUTHERN CALIFORNIA
ELECTRICAL ENGINEERING — SYSTEMS
LOS ANGELES, CA 90089-2565

DESIGN AND IMPLEMENTATION OF NOVEL OPTICAL SUBSYSTEMS FOR ENHANCING SPECTRAL EFFICIENCY, SECURITY, AND PERFORMANCE OF HIGH-SPEED WDM AND OCDMA LINKS

by

Paniz Ebrahimi

A Dissertation Presented to the
FACULTY OF THE GRADUATE SCHOOL
UNIVERSITY OF SOUTHERN CALIFORNIA
In Partial Fulfillment of the
Requirements for the Degree
DOCTOR OF PHILOSOPHY
(ELECTRICAL ENGINEERING)

December 2004

DEDICATION

To my parents,

Dr. Aram Taati and Dr. Abdol Hamid Ebrahimi

ACKNOWLEDGEMENTS

There are many people who greatly influenced my graduate school experience and without whom this work could not have been possible. I wish to express sincere appreciation to

My advisor Professor Alan Willner, for his guidance, encouragement and continuous support during my graduate studies.

My husband Hamid, who supported me and encouraged me from long before we were married. This thesis is as much his as it is mine.

Professors N. E. Bickers, T. A. Brun, P.V. Kumar, B. Gagliardi, and B. Scholtz for attending my qualification and dissertation committees and for their comments on my thesis.

Professors O. Solgaard, C.R. Menyuk, D.A.B. Miller and Kyoungsik Yu, Ivan Lima and Ray Chen for very fruitful collaborations.

Professor P.V. Kumar, Deniz Gurkan, Reza Omrani and Poorya Saghari for many fruitful discussions about OCDMA.

My colleagues in the optical communications lab where with out the help of each of them, my work wouldn't have been possible. Reza Khosravani, Michelle Hauer, Yan Wang, Deniz Gurkan and Asaf Sahin where we stayed up long hours to build the experiment and take data. Poorya Sagahri, Reza Gholizadeh, Ehsan Pakbaznia and John McGeehan for collaboration on the OCDMA experiments.

Milly, Mayumi, Gerrylin, Diane and Tim for their continual support and care.

My aunt and uncle, Mahasti and Mahmood who treated me like a daughter when I came to US for my graduate studies and thought me all the details of the new life.

My aunt Poopak and my uncle Hossein for their support for my graduate school application and support through the years.

My aunt and uncle Paran and Mehdi and my cousins Shirin and Pouya who have made my life in united states feel much more like home

My brother who has been with me with his love and support through all the steps of my life, even from far away.

I would like to express my deepest thanks to my parents, for their years of endless support and constant inspiration, for teaching me the deep values of

science from my early childhood, and for teaching me not ever to give up. I would not be here if it weren't for you.

TABLE OF CONTENTS

LIST OF FIGURES

ABSTRACT

To increase the capacity of optical links, higher bit rates, longer transmission links, narrow channel spacings and lower noise are desirable. The following projects each study a different issue to maximize throughput

- All order PMD emulator to be able to test systems and PMD compensators

Polarization mode dispersion (PMD) is one of the critical hurdles in achieving higher bit rate optical transmission. PMD is caused by an optical fiber's randomly varying birefringence and is a statistical phenomena. Since high PMD fibers already installed are not readily available and even if they were, the changes in the fiber are too slow, realistic all order emulators are needed to test the systems and PMD compensators. We investigated both experimentally and theoretically a technique to realistically emulate PMD. It is shown that: (a)the DGD of this emulator is Maxwellian-distributed over an ensemble of fiber realizations at any fixed optical frequency, and (b)the frequency autocorrelation function of the PMD emulator resembles that of a real fiber when averaged over an ensemble of fiber realizations

- Effects of PMD on the signal gain in distributed Raman amplified links

We show that polarization dependent gain (PDG) in Raman fiber amplifiers is a statistical parameter that depends on the PMD of the fiber. The PDG distribution is characterized by simulation and verified by experiment.

- Stimulated Brillouin scattering and Rayleigh scattering effects in bi-directional and narrow channel spaced Raman amplified links

We characterize the degradations due to SBS and Rayleigh backscattering in a 10Gb/s DWDM bidirectional transmission link using distributed Raman amplification for channel spacings smaller than 25GHz for different cases of signal input power and amplifier gain. We show that there is an optimum range of gain-input power combinations, governed by the SBS threshold, that permit bi-directional transmission at 12.5GHz spacing with less than 2dB power penalty.

- A 10-μs-tuning MEMS-actuated Gires-Tournois filter for use as a tunable wavelength demultiplexer and a tunable OCDMA encoder/decoder

We used a rapidly tunable wavelength-tunable GTI mux/demux with 10μs switching time to demonstrate rapid wavelength switching of data streams in a WDM system as well as code hopping in a 2D time/wavelength OCDMA system.

1. INTRODUCTION

Optical fiber communications has been growing rapidly over the past decade. The major break-through in optical fiber transmission came after invention of the Erbium-Doped Fiber Amplifier (EDFA). EDFAs, due to their wide gain band (~ 3 THz), made Wavelength Division Multiplexing (WDM) feasible.

The demand for network bandwidth is outpacing even the astounding advances of recent years. The ever-increasing fiber optic base and the acceptance of wavelength-division multiplexing (WDM) as an established technology are waiting to fulfill the enormous future potential of next-generation Internet services. The proliferation of online services and network access providers coupled with low cost computers result in exponentially-increasing numbers of customers, with increasing bandwidth demands to support multimedia and other revolutionary applications. Faster processors fuel this demand as today's computers are outdated tomorrow. More and more people spend more and more time online to perform more and more everyday tasks. Because of its high capacity and performance, optical fiber communications have already replaced many conventional communication systems in point-to-point transmission, and networks and also have been considered as a good candidate for wireless backbone.

Current research has explained how to mitigate bandwidth limiting effects for network speeds up to 10's of Gbit/s. However, in the not-too-far future speeds

approaching 100's of Gbit/s and eventually Tbit/s will be required as WDM optical networks are implemented widely. For those capacities, all the degrading effects on the optical signals in the fiber or devices need to be addressed

To fully utilize the bandwidth of the fiber and achieve a high performance, several problems need to be solved. Optical signals suffer from many effects in the fiber; including chromatic dispersion, fiber nonlinearities, and polarization mode dispersion (PMD). Although, these effects and possible solutions have been investigated both theoretically and experimentally for a while, still a lot of issues need to be addressed and better solutions need to implemented to achieve ultra-high capacity and performance systems.

2. BACKGROUND

2.1 Polarization Mode Dispersion (PMD)

An optical wave of arbitrary polarization can be represented as the superposition of two orthogonally-polarized modes. In an ideal fiber these two modes are indistinguishable, and have the same propagation constants owing to the cylindrical symmetry of the waveguide. However, in real fibers there is some residual anisotropy due to unintentional circular asymmetry usually caused by noncircular waveguide geometry or asymmetrical stress around the core as shown in Figure 2.1.1. In either case, the loss of circular symmetry gives rise to two distinct orthogonally-polarized modes with different propagation constants.

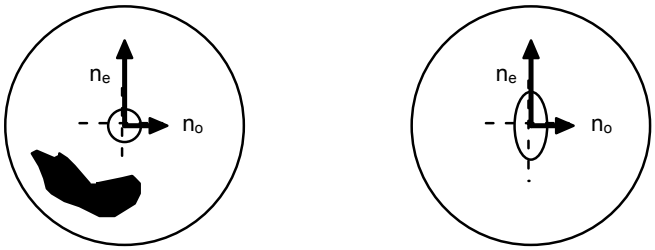

Birefringence Due to Stress

Birefringence Due to Eliptical Core

Figure 2.1.1 Origin of PMD.

The difference in propagation constants (differential phase velocity) of these two modes is responsible for polarization mode dispersion (PMD) in the fiber, and can be related to the difference in refractive indices between the two orthogonal polarization axes as

$$n_o - n_e = \beta n_o/c - \beta n_e/c = \beta \Delta n_{eff}/c \qquad (1)$$

where n_o and n_e are the effective refractive indices of two orthogonal axes, and Δn_{eff} is the differential index of refraction. The differential index of refraction is a measure of birefringence in the fiber, and is usually between 10^{-7} and 10^{-5}. The differential phase velocity indicated in equation 1 is accompanied by a difference in the group velocities for the two polarization modes. This differential group delay (DGD) which can limit the bandwidth of the fiber by broadening pulses, leads to Polarization Mode Dispersion (PMD). PMD is usually expressed in units of ps/km for a short length of birefringent fiber. Typical PMD values for these lengths of fiber are 0.1 to 1.5 ps/km [22]. This linear length dependence of PMD applies to short fibers (1 m to 1 km) where birefringence is considered to be uniform. However, PMD does not accumulate linearly along a long link of fiber. Instead, because of random variations in the perturbations along a fiber span, PMD in one section may either add to or subtract from another section of the fiber. As a result, PMD in long fiber spans accumulates in a random-walk-like process that leads to a square root of transmission-length dependence [20]. Therefore, PMD is expressed in ps/km$^{1/2}$ in long fiber spans, and atypical PMD

parameter ($\Delta\tau$) is 0.1 to 10 ps/km$^{1/2}$. The lower PMD in long spans comes at a price. Because of the temperature dependence of the many perturbations that act on a fiber, transmission properties typically vary with ambient temperature [15]. In practice this means a random, time-varying drift of polarization in the fiber. Therefore, PMD of the fiber link fluctuates randomly, causing random fluctuations in system performance. Additionally, in a cascaded fiber link, there may be many discrete components (i.e., isolators, couplers, wavelength multiplexers) which are polarization dependent due to molecular asymmetry (anisotropy) of the waveguide material. Although PMD caused by polarization dependence of a single component may be negligible, cascaded components may add significant PMD in a long link. The combined PMD-induced broadening in a long link may be up to a few tens of ps, which can degrade systems operating at ≥10 Gbit/s. In systems operating at ≥40 Gbit/s, PMD has been proved to be deleterious. In order to enable ultra-fast TDM/ WDM/ OCDMA communications over long distances of optical fiber, the remaining critical issue of PMD must be addressed and understood.

2.2 Raman Amplification

Raman amplification is based on stimulated Raman scattering (SRS), a nonlinear effect in fiber-optical transmission that results in signal amplification if optical pump waves with the correct wavelength and power are launched into the fiber[1].

A Raman amplifier uses intrinsic properties of silica fibers to obtain signal amplification. This means that transmission fibers can be used as a medium for amplification, and hence that the intrinsic attenuation of data signals transmitted over the fiber can be combated within the fiber. An amplifier working on the basis of this principle is commonly known as a distributed Raman amplifier (DRA).

The physical property behind DRAs is called SRS. This occurs when a sufficiently large pump wave is co-launched at a lower wavelength than the signal to be amplified. The Raman gain depends strongly on the pump power and the frequency offset between pump and signal. Amplification occurs when the pump photon gives up its energy to create a new photon at the signal wavelength, plus some residual energy, which is absorbed as phonons.

Raman amplifiers have become a very important part of optical communications. EDFAs revolutionized fiber optics and made it possible to regenerate the signal in the optical domain and to be able to transmit long distances all optically but Raman amplifiers enable larger bandwidths of the fiber spectrum to be used and longer transmission lengths achieved Additionally since EDFAs have isolators to prevent the EDFA to lase, the Raman amplifiers become a very good candidate for bi-directional data transmission links.

He Raman amplification process and it's advantages have been known since 1960's but in the last few years the availability of cheaper semiconductor pump lasers at the 1430-1480 nm range have made the use of Raman amplifiers economically feasible.

Raman amplifiers can be used as either lumped or distributed amplifiers. When used as distributed amplifiers they basically reduce the loss of the link instead of increasing the power of the signal at the end of fiber. In determining the length of the transmission link, the two main factors are the minimum power at the fiber where signal should be distinguishable from noise, and the maximum input power tolerable to avoid nonlinearities. In Raman amplified links, since the total loss of the link is reduced, for the same minimum power and maximum input power, longer transmission distances can be achieved. If the same length of fiber is being used, lower input powers ensure lower nonlinearites in the fiber which can increase spectral efficiency due to the reduction of FWM and XPM. Additionally Raman amplifiers have larger bandwidth than EDFAs (90nm vs. 30nm) and a smaller noise figure.

The big limiting factor of a Raman amplifiers is double Rayleigh back scattering (DRBS). This effect is actually the multipath interference between the main signal and the double Rayleigh scattered copy of it. Basically since the Raman amplification is happening through out the fiber, even the Rayleigh scattered part of the main signal is amplified enough for it's own Rayleigh scattered signal to

be high enough to cause crosstalk with the main signal at the detector. The main problem is that since both the main signal and the crosstalk are at the exact same wavelength, eliminating the crosstalk is not easy. This effect limits the gain of the Raman amplifiers. Hence EDFAs are still needed in the links and the most efficient way is to use both amplifiers in long distance optical communication links.

2.3 Optical Code Division Multiplexing (CDMA)

Optical code-division multiple access (OCDMA) has emerged as an attractive means for providing secure digital communication channels between multiple users at the physical layer. The concept of CDMA originally surfaced as a means for multiple users to share the limited bandwidth of the atmosphere for RF communication systems. In an optical fiber network, however, raw fiber bandwidth is not at a premium and CDMA is attractive for different reasons. OCDMA allows multiple users to send data bits over the network asynchronously without any centralized network control, unlike time-division multiple access (TDMA) or wavelength-division multiple access (WDMA) systems in which a network controller must dynamically assign timeslots or wavelengths to each user, respectively. Furthermore, with the appropriate choice of address codes in a CDMA system, each user will only be able to decode the bits destined for their node, enabling secure communication.

In an OCDMA system each bit is divided into ***n*** timeslots, called "chips." A codeword is created by illuminating some of these chips using short optical pulses while leaving the remaining chips empty. The weight, ***w***, of a codeword is equal to the total number of illuminated chips. In most OCDMA schemes, all codeword have the same weight, although some multi-weight codeword schemes have been presented. Each node, or user, in the network is assigned a unique codeword. To send a "1" bit, the transmitter simply sends the appropriate codeword while a sequence of all-empty chips represents a "0" bit. The transmitted codeword from each user are broadcast to all other nodes in the network. The receivers in the network are optical correlators configured to provide an autocorrelation peak whenever the incoming chip-stream matches the "stored" codeword it is programmed to recognize, and produces a cross-correlation output for all other codewords. Thus, to effectively implement an OCDMA system, the choice of the codeword set is critical and must possess certain properties, some of which are in contrast to each other, meaning that the optimal codeword properties are governed by the needs of the specific network (security level, number of users, etc.)[18].

The weight of the codeword should be as large as possible to provide a large received autocorrelation peak relative to the cross-correlation outputs due to all other received codeword. This maximizes the signal to interference ratio at the receiver.

Whenever the desired codeword is shifted in time by any number of chips, the autocorrelation output is small compared to the code weight, guaranteeing a continuously low correlator output whenever the receiver is not synchronized with the transmitter. This enables the receiver to operate asynchronously without the need for a global clock.

The cross-correlation output for any two distinct codeword in the set must be small, ensuring a minimal level of interference from the presence of other user's codeword in the received signal.

To maximize the number of simultaneous users accommodated by the network, the length, $\boldsymbol{n}$, of the codeword should be long while the weight, $\boldsymbol{w}$, should be small.

The families of codeword that meet the above requirements are termed "Optical Orthogonal Codes (OOC)." Since the receivers in an OCDMA system must extract their codeword in the presence of all the other user's codewords, the dominant source of noise is due to the interference of the other user's signals and is termed multiple access interference (MAI). Thus, the codeword sequences must be intelligently selected to mitigate this interference term to ensure a low bit-error-rate (BER) for the received signal. The total number of codewords in a

family is termed the size, or cardinality, of the code and, for a one-dimensional OCDMA scheme as described above, is defined as:

$$\Phi(n,w) \le \left(\frac{n-1}{w(w-1)} \right) \qquad \text{1-dimensional code size}$$

2-Dimensional OCDMA: Hybrid wavelength hopping - time spreading codes

In order to increase the number of simultaneous users in a conventional OCDMA network, the length, *n*, of the code words should be large, meaning that each bit must be divided into numerous, short-period chips. For large *n*, this places a prohibitively large demand on the speed of the electronic, and even photonic, devices needed for transmission of the coded bit-streams.

Fortunately, the optical domain allows us to utilize an added degree of freedom: the wavelength domain. By encoding each illuminated chip with a unique wavelength, the number of allowed code words increases without the need for more chips per bit. A single codeword of this 2-dimensional coding scheme is

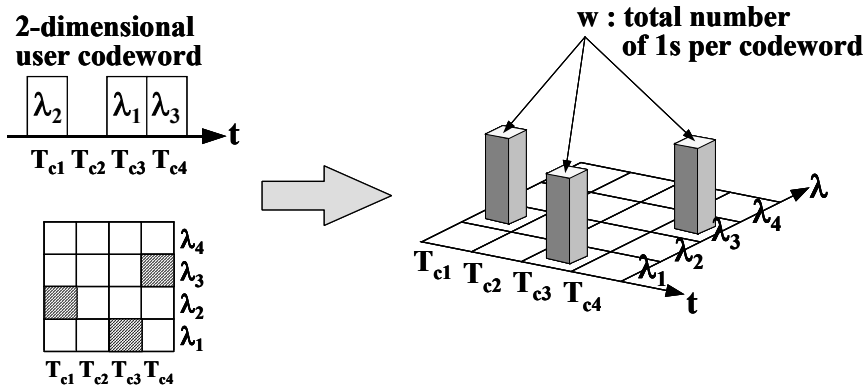

Figure 2.3.1 Two dimensional OCDMA System Three ways to envision a 2-dimensional codeword using both the time and wavelength domains. Each bit sent is coded by dividing it into n chips, each of period T_c. A codeword is created by transmitting a 1 during some of these chip times and not others. The weight of the code is the total number of "1" chips per codeword. By additionally placing each illuminated chip on a different wavelength, a 2-dimension wavelength-hopping, time-spreading code is created that significantly increases the number of users that may be accommodated by the OCDMA system.

illustrated in Figure 2.3.1. Note that it is now possible to have the same time-sequence for more than one user since different wavelength combinations may be used for each. The increase in the number of simultaneously allowed users in this scheme is quite remarkable. For example, if a one-dimensional code with *n*

= 1000 chips and weight, $w = 9$ is able to support a maximum of 13 users with time-spreading on one wavelength is expanded to include four wavelengths, then the maximum number of simultaneously allowed users increases to 1300 [30]. An additional advantage of using 2-D codes is the increased security achieved. L. Tancevski, et al, show in [28] that by using prime-hop sequences (a robust set of code words with the properties listed above) in which 11 out of a set of 33 possible wavelengths are used for each codeword, it would take an intruder 270 years to test all possible codeword combinations at an impressive test rate of 10^7 combinations per section.

3. DEGRADING EFFECTS FOR DIFFERENT SIGNALS AND SYSTEMS AND TECHNICAL SOLUTIONS

3.1 Polarization Mode Dispersion Emulator

3.1.1 Introduction

Polarization mode dispersion (PMD) has recently emerged as one of the next critical hurdles in achieving high-performance optical transmission systems and networks. PMD is caused by the optical fiber's randomly varying birefringence. To first order, PMD can be represented by a differential group delay between two principal states of polarization (PSP) [19]. For a fixed PMD, DGD is a random variable that has a Maxwellian distribution [7].

Although present-day fibers have PMD values ~ 0.1 ps/km$^{1/2}$, much of the fiber installed throughout the 1980's has PMD values ranging from 1 to as high as 10 ps/km$^{1/2}$. Since all the deployed systems must first be proven viable in the laboratory, a critical problem for designers of high-performance systems is to measure performance degradations due to high-PMD fiber spans. Unfortunately, high-PMD fiber is not commercially available, and it is hard to use it to rapidly explore a large number of different fiber realizations, as is required to determine the distribution of the penalties due to PMD.

A fairly well known technique of quasi-PMD emulation is to connect several short spans of polarization-maintaining (PM) fiber with some fixed angular offset between each section. However, this approach does not guarantee that the multi-PM-section module has the PMD characteristics of a real fiber and may provide a false measurement. True PMD has a Maxwellian distribution of the DGD, and this distribution has not been shown to hold for most previously described emulators. It would be highly advantageous for the optical communications community to have a PMD emulator that closely simulates the embedded fiber base.

We investigate a new technique to accurately emulate PMD. We demonstrate that 15 sections of PM fiber with randomly rotatable connections produce an almost ideal Maxwellian distribution of the DGD, while the distribution for a significantly smaller number of sections or for 15 sections with fixed connections is inadequate.

3.1.2 System Model and Experimental Set-Up

Figure 3.1.1. shows the set-up of our PMD emulator. We have used different sections of PM fiber (Fiber Core, HiBi, Bow-Tie) connected by rotatable key FC connectors. By using rotatable connectors, the polarization axes of the two adjacent fibers can be rotated with respect to each other, and many realizations of

concatenated PM fibers can be obtained. The average length of PM fibers has been chosen ~ 7 meters with a 20% Gaussian deviation [21]. The beat length of

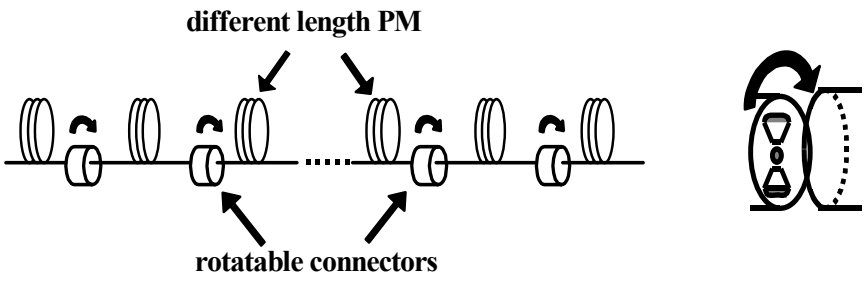

Figure 3.1.1 Experimental setup of the PMD emulator, with up to 15 sections of PM fibers of varying lengths

the PM fibers are ~ 1.2 mm at 633 nm and scales for higher signal wavelengths. Therefore, by using 15 sections of PM fiber, 40 ps PMD is generated. The fiber lengths for the 15 sections are 5.1, 6.8, 8.6, 7.4, 6.3, 6.7, 10.0, 8.6, 5.4, 7.2, 6.9, 7.1, 6.1, 7.4, 4.6 meters. The total loss for the emulator is 6-10 dB, depending on the angles between the PM fiber sections. The PDL has been measured to be <0.2 dB. The DGD value is measured using the Jones Matrix method.

It is possible to emulate different realizations of the system by sweeping over different frequencies after fixing the angles between the fiber sections. In Fig. 3.1.2,we show the results of doing that for 3 and 15 sections. With 3 sections, we find that the distribution of the DGD is far from Maxwellian. Even with 15 sections, the results are not adequate in most cases, although there are some cases that closely resemble a Maxwellian distribution. Moreover, a substantial troublesome correlation persists between the different frequencies with an

average level of 10%, as shown in Fig. 3.1.2.(c). Thus, we conclude that it is not reliable to use different frequencies to emulate different fiber realizations.

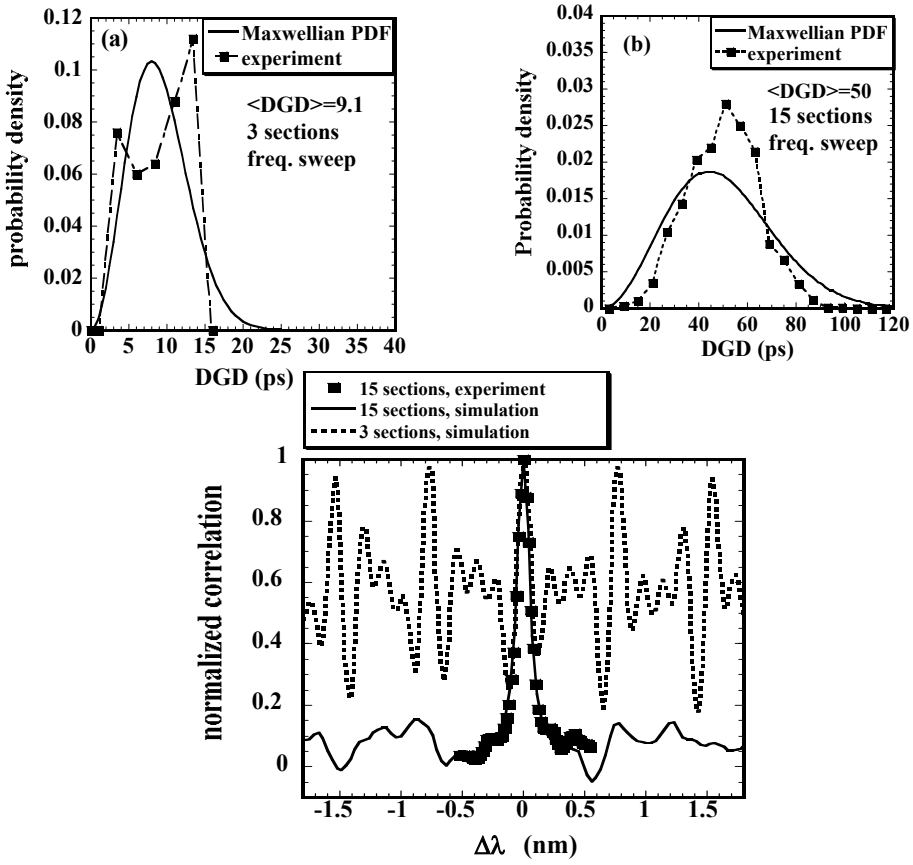

Figure 3.1.2 (a) DGD distribution for optical frequency sweep using a 3-section PM fibers emulator, (b) same distribution using 15-section PM fiber emulator, (c) correlation function for PMD vector of 3-section and 15-section (theoretical and experimental) emulator.

3.1.3 Theory of PMD Emulators

From a theoretical standpoint, the best emulator would have polarization scramblers between the sections of PM fiber that could make an arbitrary rotation on the Poincare sphere. In this case, it is possible to obtain an iterative analytical expression for any number of sections of any length, as shown in Equation (1):

$$f_{\Delta\tau_{n+1}} = \frac{\Delta\tau_{n+1}}{2a} \int_{|\Delta\tau_{n+1}-a|}^{\Delta\tau_{n+1}+a} \frac{f_{\Delta\tau_n}(\Delta\tau_n)}{\Delta\tau_n} d\Delta\tau_n \qquad (1)$$

where a is the DGD of the (n+1) section. In Fig. 3.1.3, we show the distributions

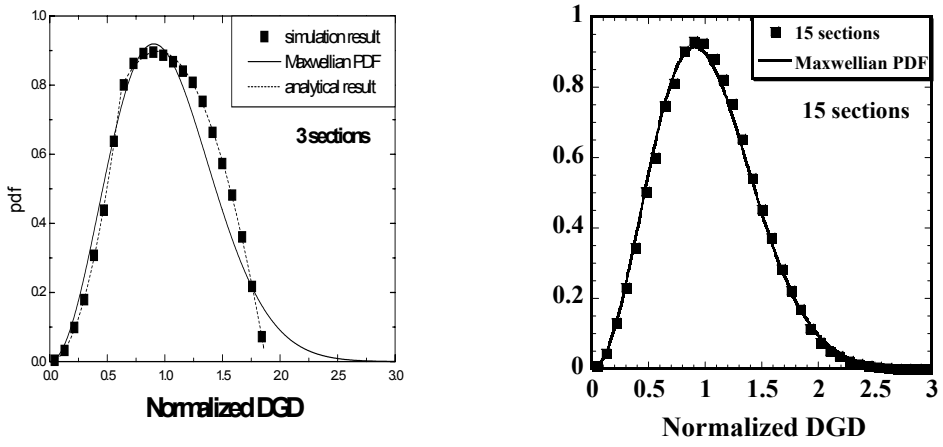

Figure 3.1.3 DGD distribution for a (a) 3 and (b) 15 section PMD emulator with polarization scrambling between each section. Monte Carlo simulations and analytical results are included.

for 3-, and 15- section emulators.

In practice, an emulator with polarization scramblers is hard to build. So, in our experiments we used rotatable connectors, shown in Fig. 1, that only changes the polarization orientations but not their relative phase. In this case, we do not have an analytical expression for more than three sections, but we obtained the DGD

distribution functions using Monte Carlo simulations based on the coarse step method [12].

3.1.4 Experimental Results and Comparison to Theory

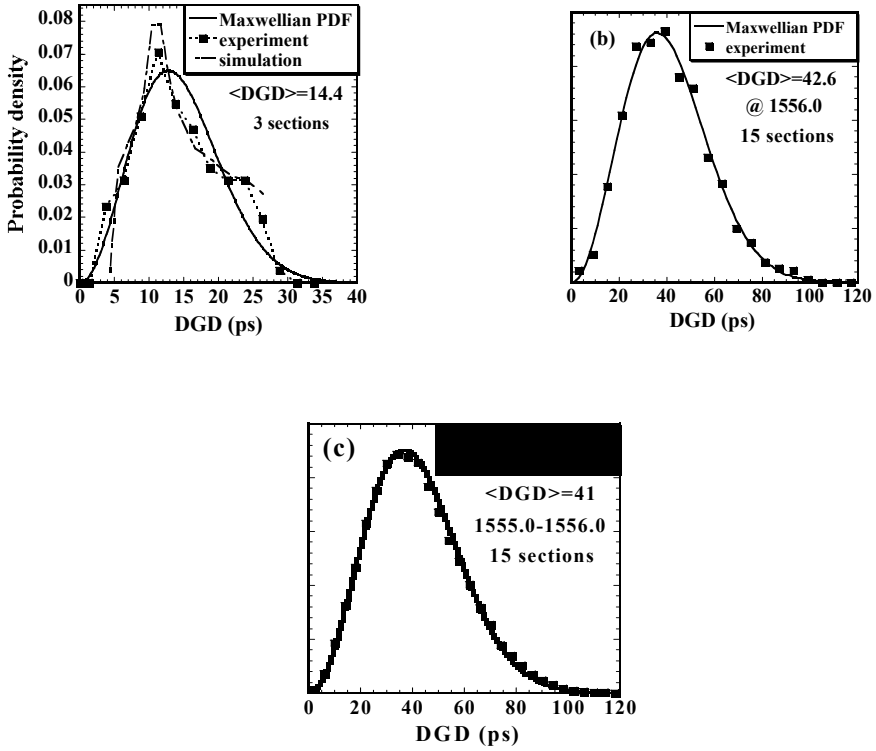

Figure 3.1.4 a) DGD distribution for different angle realizations of a 3-section of PMD emulator, simulation and experiment results, b) same distribution for 15-section emulator, c) same distribution including all frequencies in the range of 1555-1556.

We began our studies by investigating a 3-section emulator in which we rotate the connectors. Figure. 3.1.4a shows the DGD distribution for 3-section emulator when the angles between the PM fibers are rotated randomly (uniform

distribution). It is clearly seen that 3-section PM fiber emulators cannot mimic the real fiber behavior.

We increased the number of sections to 15 and measured DGD for 1035 different realizations by randomly rotating the angles between the fibers. At the same time we swept the wavelength for 1 nm in each realization. Figure 3.1.4b shows the DGD distribution at 1556.0 nm. As is apparent, a good DGD distribution is obtained for each individual wavelength. Figure 3.1.4c shows the distribution of the whole data (1 nm sweep, 1035 different realizations). An excellent match with Maxwellian distribution is shown. And even with only 400 different realizations a good distribution over the Poincare sphere was seen.

3.2 Statistics of Polarization Dependant Gain in Raman Fiber Amplifiers due to PMD

3.2.1 Introduction

With the recent availability of high power pump lasers, Raman amplification has become feasible for commercial DWDM fiber-optic communication systems. Raman fiber amplifiers are highly attractive for their low equivalent noise figure and wideband gain. However, the Raman gain coefficient is polarization sensitive and can be up to 10 times higher when the signal and pump polarization states are parallel rather than perpendicular [25]. Previous studies of this polarization dependent gain (PDG) investigate its relationship with the polarization mode dispersion (PMD) of the fiber [11], and the degree of the polarization (DOP) of the pump laser [33]. These studies show that when the average PMD of the fiber becomes high enough, or if the pump DOP is very low, then the PDG becomes negligible. But these studies do not investigate the statistical behavior of the polarization dependant gain.

There are two ways of characterizing polarization sensitivity in Raman amplifiers. One is to measure the PDG at a given point in time, which is determined by varying either the pump or signal polarization and recording the difference between the maximum and minimum gains. Alternatively, one can monitor how the instantaneous gain varies over time due to both PMD induced

variations and changes to the signal's input state of polarization (SOP). In this paper we investigate the statistical characteristics of both of these parameters theoretically and experimentally.

Since PDG is greatly reduced for counter-propagating pump schemes, we use a co-propagating configuration in our experimental setup to magnify the polarization effects. Co-propagating amplifiers have certain improved amplification characteristics and may be useful in some system applications [25], and for these, a quantitative understanding of PDG statistics may be critical. Our results show how the mean and standard deviation of the PDG decreases with increasing values of PMD.

3.2.2 Experimental setup

Figure. 3.2.1 depicts the experimental setup. The Raman amplifier consists of 10 km of unspooled dispersion shifted fiber. The input pump power is 205mW and the average gain is 3.4 dB. The signal passes through a computer controlled polarization controller to vary the signal's input SOP. The switch in the pump path is used to "turn off" the pump for gain measurements. The pump and signal are separated at the output where the signal power fluctuations are monitored with an optical spectrum analyzer (OSA).

Within the amplifier, 11 polarization controllers (PCs) are placed at approximately 800m intervals. By changing these PCs between measurements, we induced random variations in the polarization mode coupling within the transmission fiber that would otherwise only occur over a long period of time.

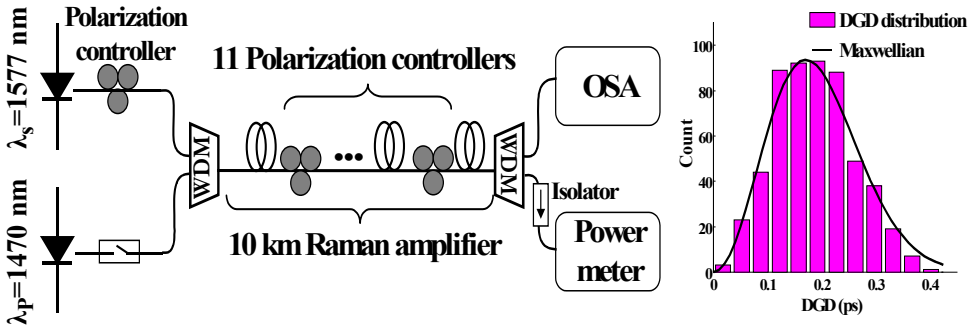

Figure 3.2.1 Raman amplifier setup and measured DGD distribution; <DGD>= 0.19ps, PMD=0.06ps/km$^{1/2}$.

We verified this technique by taking 500 samples of instantaneous differential group delay (DGD) at our signal wavelength while randomly changing the PCs between measurements. The resulting DGD distribution (Figure 3.2.1) closely approximates the expected Maxwellian and yields an average PMD of 0.06 ps/km^{½}. It should also be noted that the PDL of our setup is ≤0.33dB, which is about 1 dB less than our average PDG.

3.2.3 Results

Figure. 3.2.2a shows the measured PDG distribution. The 11 PCs were varied randomly between each of the 500 samples. During each measurement, the output signal power was monitored while the input signal SOP was varied randomly. The maximum achieved power fluctuation determines the PDG since the average

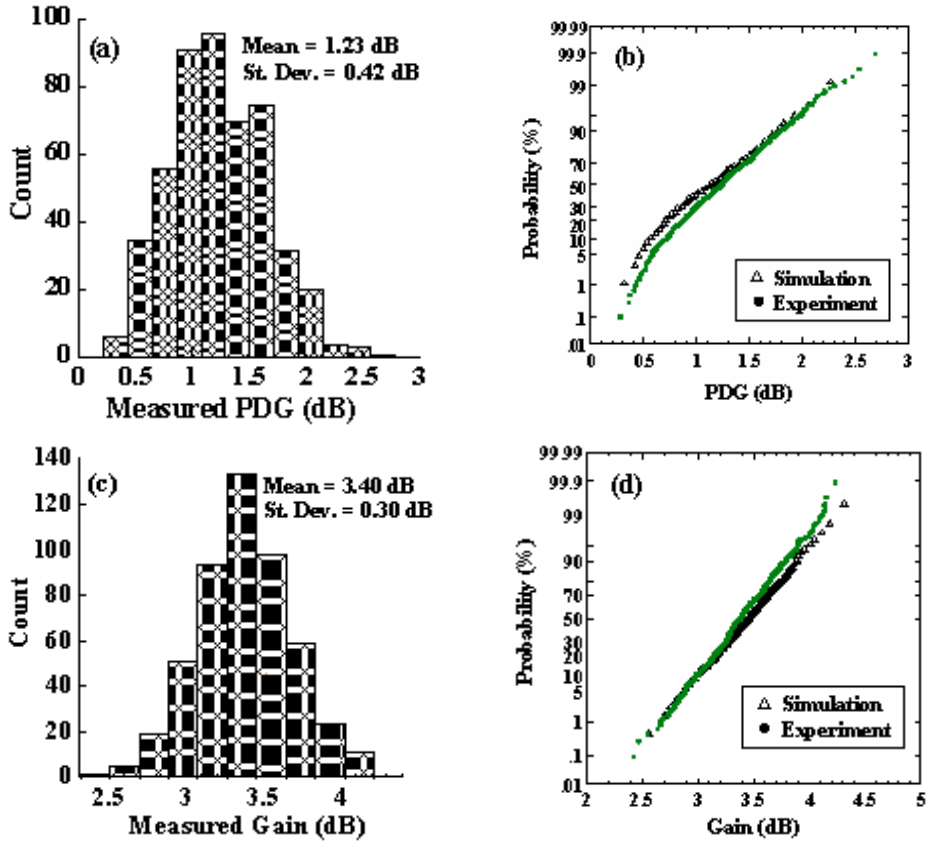

Figure 3.2.2 (a) Measured histogram of PDG, (b) simulated vs. experimental cumulative distribution functions of PDG; (c) and (d) show the same plots for the Raman gain (for PMD=0.06 ps/km$^{1/2}$).

Raman gain, which was also measured at each data point, remained constant at 3.4±0.15 dB (variation due to PDL). To further verify our measurement technique, another 500 samples were taken without changing the 11 PCs at all (over a period of only four hours to avoid the natural evolution of polarization

coupling within the fiber). The resulting PDG remained constant within ±0.2 dB, adding validity to our method. Figure 3.2.2b shows the cumulative distribution functions (cdf) for the measured and simulated PDG for 0.06 ps/km$^{1/2}$ PMD. Note the simulated and experimental results closely agree. Similarly, figures 3.2.2c and 3.2.2d show the measured and simulated distributions of the instantaneous Raman gain. Again, the simulated and experimental results are in agreement.

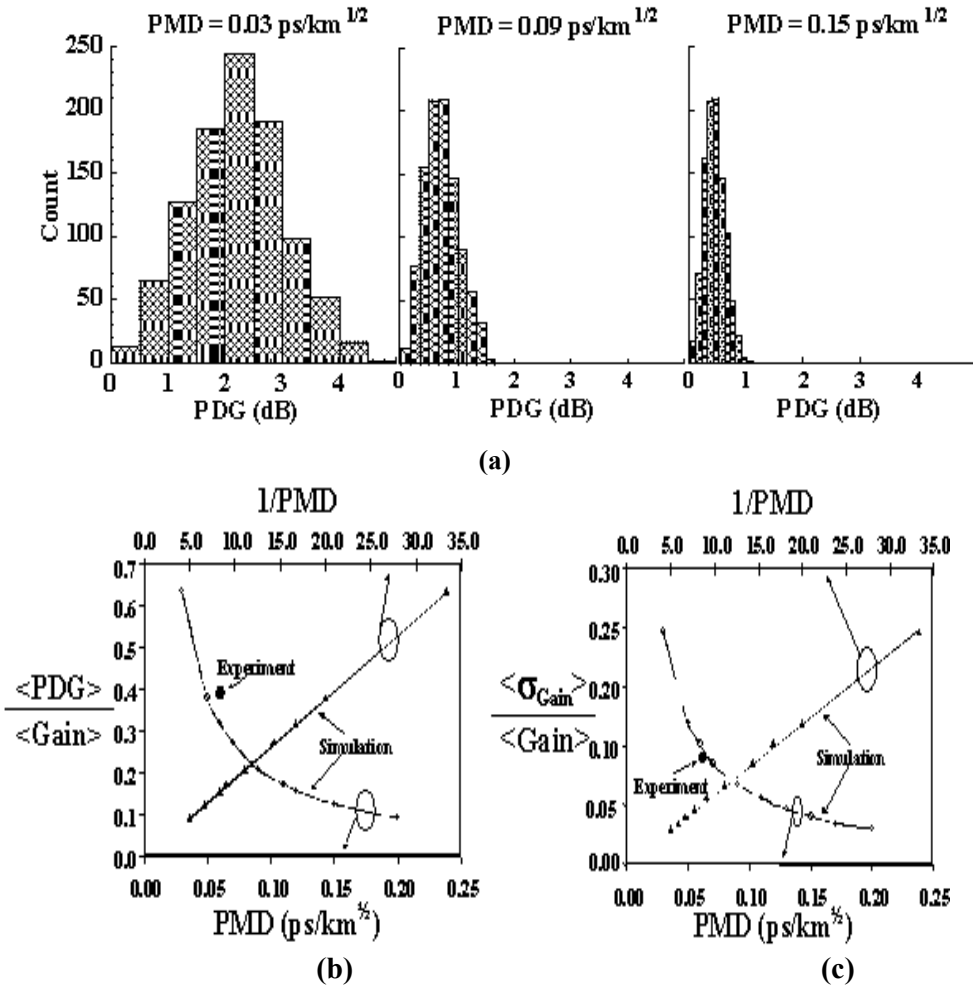

Figure 3.2.3 (a) Histograms showing how the mean and standard deviation of the Raman PDG decrease as the PMD is increased from 0.03 to 0.09 to 0.15 ps/km^{½}; (b) and (c) show the mean PDG and the standard deviation of the Raman gain versus PMD (and 1/PMD) for a 10-km Raman amplifier (where the PDG and gain are normalized to the average gain).

Since our experimental results are presently limited to only a single PMD value (we are looking for higher PMD fibers to further our experiments), the simulation was used to investigate how the PDG statistics vary for different values of PMD. Our simulation models a fiber with PMD as a series of 1000 equal length sections with random polarization mode coupling between them. The Raman gain of each

section depends on the relative polarizations of the signal and pump. Figure 3.2.3a shows that even modest increases in the PMD reduce both the average and spread of the PDG distribution. Figure. 3.2.3b shows the normalized variation of the mean PDG versus PMD.

The results show that a total PMD of 0.66 ps ($0.2ps/km^{½}$ x $(10km)^{½}$) is enough to reduce the mean PDG to as low as 10% of the average gain. Figure. 3.2.3c shows the normalized variation of the standard deviation of the Raman gain versus PMD. Also note that the constant slope in Figure. 3.2.3b shows that the product of the mean PDG and the PMD of the link remains constant, as does σ_{Gain} x PMD (Figure. 3.2.3c)[5].

3.3 Effects of SBS and Rayleigh Scattering in Densely-Spaced Bidirectional Transmission using Raman Amplification

3.3.1 Introduction

A key goal of dense wavelength-division-multiplexed (WDM) optical transmission systems is to efficiently use the available bandwidth and pack the channels as close together as possible. However, the following impairments can occur when channels are spaced very close to each other: (i) high cross talk and high induced chirp due to wavelength drifts as well as limitations in optical filtering and demultiplexing technology, and (ii) increased nonlinear effects [3]. For example, it may be desirable to transmit many 10-Gb/s channels that are spaced only 12.5 GHz apart, but this tends to severely push the technology envelope. One potential solution for high spectral efficiency is to implement a bidirectional transmission link over a single fiber for which the WDM channels are interleaved in the forward and backward directions. Certainly, the requirements for the filtering technologies would be significantly relaxed. Furthermore, most of the nonlinear effects occur when channels co-propagate, and these would also be reduced using this method.

A bidirectional transmission link could use erbium-doped fiber amplifiers (EDFAs). However, EDFAs are inherently unidirectional devices, requiring either two EDFAs at each amplifying site or a unique interleaver configuration

[9]. A potentially more straightforward implementation is to use Raman amplification in the transmission fiber itself, for which bidirectional transmission is more compatible. Moreover, nonlinear effects can be better controlled using distributed Raman amplification (DRA) [27]. Two of the main deleterious effects for close bidirectional channel spacings are Rayleigh back reflection and stimulated Brillouin scattering (SBS). For signal powers above a threshold, SBS causes part of the signal to be reflected and down shifted by ~11 GHz. This becomes a source of inter-channel crosstalk since the reflected wave is downshifted into the band of the counter propagating, longer wavelength channel [29]. These backscattered signals will also be amplified inside the fiber causing a different effect than in a conventional EDFA amplified system.

We demonstrate 10 Gb/s bidirectional transmission over an 80-km dispersion-compensated SMF fiber link using bi-directionally pumped Raman amplification. We measure the Rayleigh and SBS degrading effects that occur for channel spacings less than 25 GHZ for different Raman gains and input signal levels. No penalty is seen for channel spacings 25 GHz and larger. We show that for gains up to 17 dB the Rayleigh degradation decreases with gain. And in order to avoid the SBS penalty at 12.5 GHz spacing, the highest signal power inside the fiber should be designed to be less than the SBS threshold. In this case, transmission with less than a 2 dB power penalty can be achieved at 12.5 GHz spacing.

3.3.2 Experimental setup

Two 10 Gb/s NRZ channels, modulated with a 2^{23}-1 PRBS bit stream, are launched from opposite directions into 80 km of SMF fiber with a loss of 0.23 dB/km (Figure 3.3.1). 12 km of DCF (-1350 ps/nm) is used before the receiver to compensate for the fiber chromatic dispersion. Throughout the experiment the

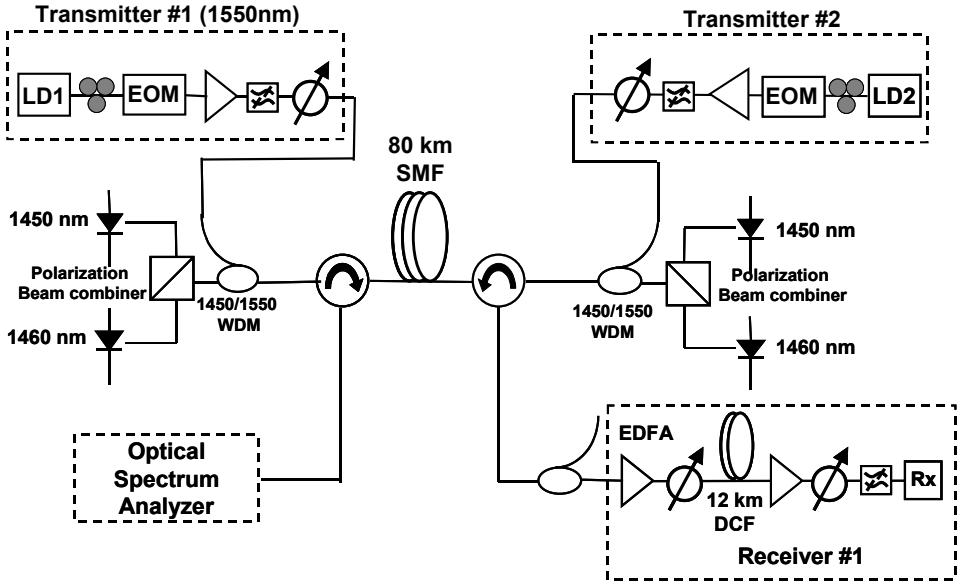

Figure 3.3.1 Experimental setup for two 10 Gb/s NRZ data streams bidirectionally transmitted through the bidirectionally pumped distributed Raman amplifier.

optical input power to the DCF is kept constant at –2 dBm to maintain the same amount of DCF transmission degradation for all measurements. The channel spacing is monitored using optical heterodyning.

At both ends of the SMF, two pump lasers at 1450 nm and 1460 nm are

polarization combined to depolarize the pump sources and minimize the polarization dependant gain of the Raman amplified channels. Frequency-locked pump lasers are used to reduce the pump–signal relative intensity noise. A maximum of 18 dB gain is obtained with a total pump power of 820 mW (205mW maximum per pump). Balanced bidirectional pumping is used to ensure

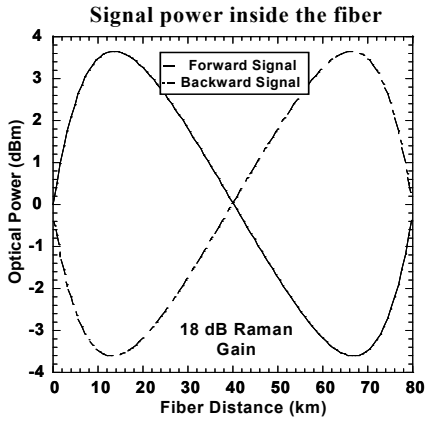

Figure 3.3.2 Signal power inside the fiber for balanced pumps and 18 dB gain (simulation results).

the same gain and signal profile for both directions. Bidirectional pumping has been shown to introduce the least amount of double Rayleigh back scatter (DRBS), and DRBS is the main limiting factor for applying higher Raman gains to the amplifier [16]. Figure 3.3.2 shows the simulation results for the optical signal power in the fiber [2].

3.3.3 Results

The reflected power of channel 1 is measured versus input power for different Raman gains to compute the SBS threshold (Figure 3.3.3a). A second modulated counter propagating channel is present at –12.5 GHz spacing and acts as an SBS

"seed" which reduces the SBS threshold. The measured SBS threshold, in terms of input signal power, versus Raman gain is shown in figure. 3.3.3b. However, in a DRA, the maximum signal power is not at the input, but instead occurs at some

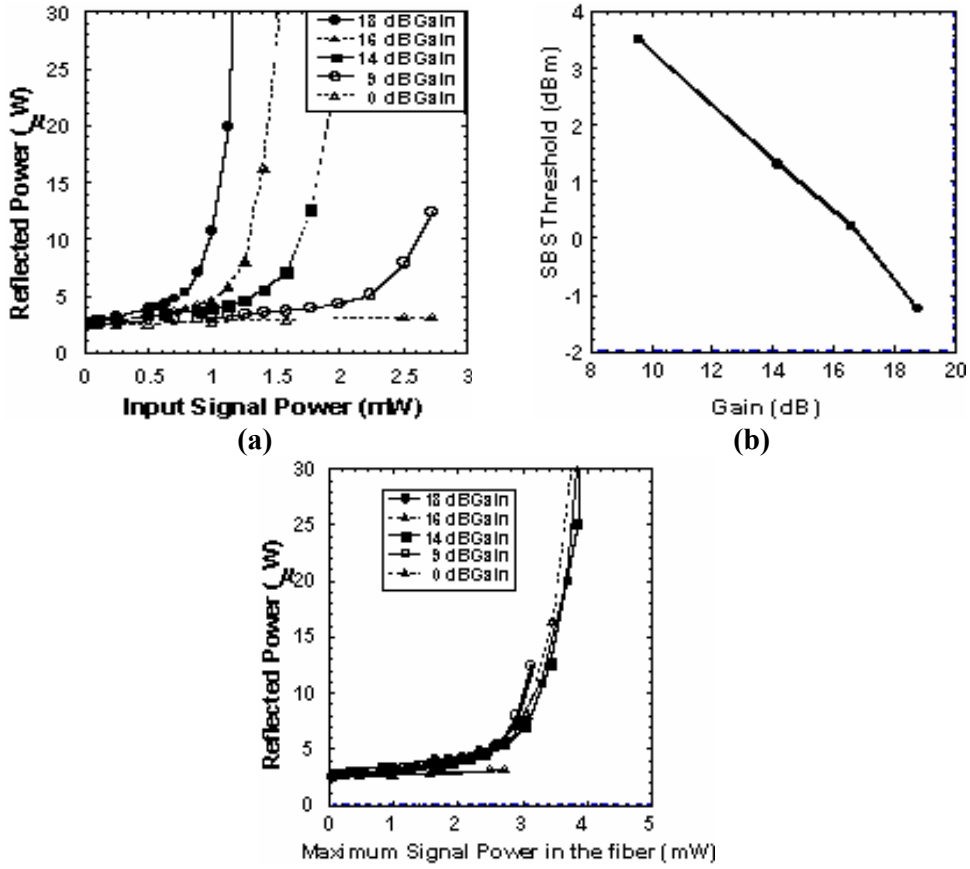

Figure 3.3.3 (a) Channel 1 reflected power vs. input power when a seed signal is present at –12.5 GHz (both modulated at 10 Gb/s NRZ). (b) SBS threshold vs. amplifier gain in terms of input signal power. (c) The reflected power vs. the maximum signal power in the fiber.

distance within the fiber and it is this power that will determine whether the SBS threshold is being exceeded. In figure 3.3.3c, the reflected power is plotted versus the maximum signal power in the fiber for various gains. It can be seen that the SBS threshold is reached whenever the maximum power in the fiber

exceeds ~3 mW for any gain. This indicates that for bidirectional DRAs, the SBS threshold is actually gain independent and only depends on the maximum signal power inside the fiber.

Figure 3.3.4 shows the power penalty versus bidirectional channel spacing for

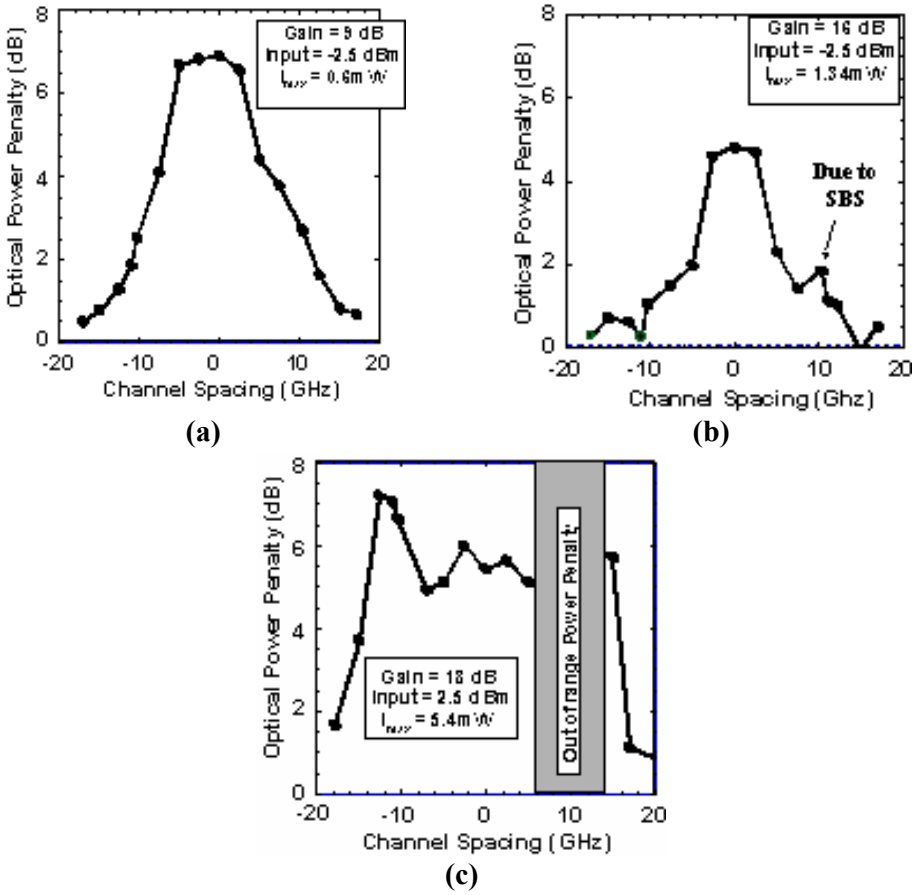

Figure 3.3.4 Power penalty vs. channel spacing for 3 different cases in the link: (a) No SBS effect, only Rayleigh is degrading the system. (b) Small SBS degradation occurs at ~11 GHz due to SBS and no SBS effect is seen at 12.5GHz. (d) Extreme SBS degradation.

three cases of input power and Raman gain, where the maximum input power in the fiber is increased in each successive case. Channel 1 is fixed at 1550 nm

while channel 2 is moved from –20 to +20 GHz relative to channel 1. For case 1 in figure 3.3.4a with a maximum power of 0.6 mW, no SBS penalty near 11 GHz is seen, and the penalty due to Rayleigh backscatter around 0 GHz is ~7 dB. Successful transmission at 12.5 GHz spacing is achieved with less than 2 dB penalty. In figure 3.3.4b, with a maximum power of 1.34 mW, a 0.5 dB degradation due to SBS is seen near 10 GHz, and still the penalty at 12.5 GHz is less than 2dB. In the high gain, high input power case (max power = 5.4 mW), SBS causes an immeasurably large penalty around 11 GHz and that extends over an unexpectedly wide bandwidth of ~8 GHz. A 7.2 dB penalty is also seen at –12.5 GHz and acts as a seed for the power transition from channel 1 to channel 2.

An optimum gain–input power combination for 12.5 GHz spacing can be derived from figure 3.3.5. Figure 3.3.5a shows the single channel degradation and figure 3.3.5b shows the penalty for 12.5 GHz bidirectional spacing. It can be seen that a minimum penalty is achieved for various gain-input power combinations. As the input power is continually increased above the penalty minimum, the SBS

threshold is exceeded and the penalty of the monitored channel is degraded so severely that error free transmission can no longer be achieved. When the second channel is placed at -12.5 GHz, the degrading effects can be still seen in the

monitored channel. This figure shows that when the signal power is changed from –5 to –10 dBm (for 15 to 18 dB gain), less than 1 dB power penalty will occur. This range also shows the capability to achieve longer distance

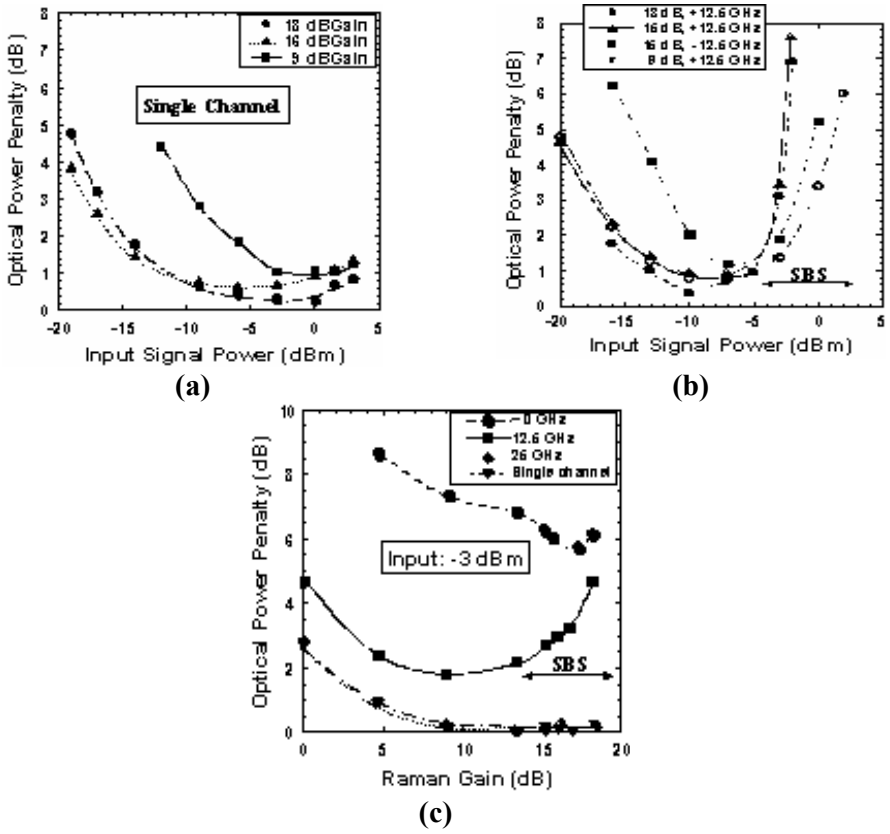

Figure 3.3.5 (a) Power penalty vs. input power for single channel transmission and (b) for bidirectional transmission at +12.5 and -12.5 GHz channel spacing. (c) Penalty vs. gain for single and bidirectional channels at ~0 GHz, 12.5 GHz, and 25 GHz spacings.

transmission with the same pumps. In Figure. 3.3.5c, the two channels were overlapped (~0 GHz spacing) and the degradation due to Rayleigh backscattering decreased with increasing gain. No degradation is seen for the case of 25 GHz bidirectional channel spacing [6].

3.4 A 10-μs-tuning MEMS-Actuated Gires-Tournois Filter for use as a Tunable Wavelength Demultiplexer and a Tunable OCDMA Encoder/Decoder

Wavelength multiplexers and demultiplexers are staples of nearly all wavelength-division-multiplexed (WDM) systems and networks. Traditionally, muxes have been static devices, with temperature tuning producing slow changes over small wavelength ranges. Almost since the first availability of static muxes, there has been a keen desire for a rapidly-wavelength-tunable version of the mux. Rapidly-tunable muxes can have wide-ranging applications, including (i) enabling reconfigurable WDM networking, and (ii) enabling tunable encoders/decoders for rapid code hopping in time/wavelength 2D optical code-division-multiple-access (OCDMA) systems, thereby adding to both quality-of-service as well as security.

There are precious few results published on tunable muxes. One recent approach to a rapidly-tunable mux is a 1xN MEMS-actuated Gires-Tournois Interferometer (GTI) [32] that uses a programmable micromirror array in place of the back reflection plane of the traditional GTI structure. Functionally, the GTI acts exactly like a tunable array waveguide grating (AWG) [4], in which the output ports exhibit a cyclic behaviour with respect to wavelength, i.e., for an N port GTI demux, the 1st wavelength comes out of port 1, the Nth wavelength comes out of port N and (N+1)th wavelength comes out of port 1, too. After tuning, the

(N-1)th wavelength emanates from output port N, the Nth wavelength emanates from port 1, and N+1th emanates from port 2. In our prototype device, the crosstalk between adjacent ports was 8 dB and the MEMS mirror tuning speed was approximately 10 μs. Although basic device measurements were published [32], no systems-level research has been reported.

In this paper, we demonstrate system level performance and rapid switching of the 1x3 wavelength multiplexer / demultiplexer based on a Gires-Tournois interferometer (GTI) with a tunable center wavelength. Group Delay Ripple (GDR) measurements have also been performed on the GTI and show <5ps GDR. Less than 0.5 dB power penalty is observed for 10 Gb/s data propagating through the demux.

Additionally, since cyclic frequency shifts of an asynchronous optical orthogonal codes of a 2D OCDMA system also result in orthogonal codes [14], this tunable Demux is a simple way to accomplish code hopping. Code hopping in an OCDMA system can increase the security since the eavesdropper will need to find the sequence of the hopped code in addition to the code itself. Code hopping has also been suggested for maintining a quality of service since tunable encoders/decoders allow a user to hop to a new code when the Multiple Access Interference (MAI) from other users is degrading the received signal quality. The MEMS GTI can be used to perform code hopping with significant advanatages (speed and simplicity) over other potential techniques which employ temperature

tuned FBGs and/or switching between delay lines. We experimentally perform code-hopping for a 2D OCDMA system using the GTI .

3.4.1 Using the GTI as a high speed switch

Each output port of the demux exhibits a periodic filter spectrum. By changing the voltage applied to the electrostatic MEMS actuator, we can change the vertical positions of micro-mirrors, and therefore introduce the phase shift of

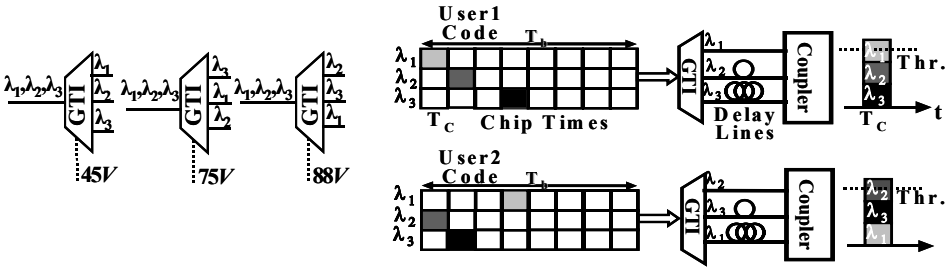

(a) (b)

Figure 3.4.1(a) By changing the voltage connected to the MEMS structure, the Demux output wavelength order gets a cyclic change. The switching speed is 10μs and the Demux bandwidth is 30nm. The FSR can also be tuned from 0.6nm – 1.2nm. (b) The cyclic shift of the GTI can be used for hopping between orthogonal OCDMA codes

incident optical beam. This phase shift is translated into the cyclic shift of the output interference pattern at the location of the output fiber array [32]. For example, the 3rd wavelength shifts from the port 3 to the port 1, the 1st wavelength shifts from the port 1 to the port 2 and so on (figure 3.4.1a).

Figure 3.4.2a shows the switching process. A single wavelength, modulated with 2Gb/s data is transmitted through the demux. By applying a voltage that switches between two different

voltages at a rate of 15 kHz, the output port for the incoming data is switched from port 2 to 1. The figure shows approximately 10μs switching speed. It was observed that the bits are not degraded during the transition but their peak to peak value changes. Crosstalk of 5-8 dB was measured in the ports in the off position, and a typical insertion loss was 11.5 dB. The main causes of high insertion loss and crosstalk are the misalignment between the components and free space coupling. Theoretically, the insertion loss and crosstalk can be further improved by using a graded beam splitter with a varying beam splitting ratio and increasing the number of micro-mirrors (currently 6). The simulation results in [32] show that the insertion loss is as low as ~3 dB and the crosstalk as good as 13 dB.

We also characterized the group delay ripple across the filter passband as shown in figure 3.4.2b. The peak-to-peak ripple remains below ~5 ps within the filter bandwidth and has a flat slope on average indicating that the filter effectively induces no chromatic dispersion. The GDR was measured using modulation phase shift method with f_{mod} = 1 GHz and λ_{step}= 0.01nm.

Figure 3.4.2c shows the BER measurements of each of the ports (with continuous transmission through the ports). Less than 0.5 dB power penalty was measured.

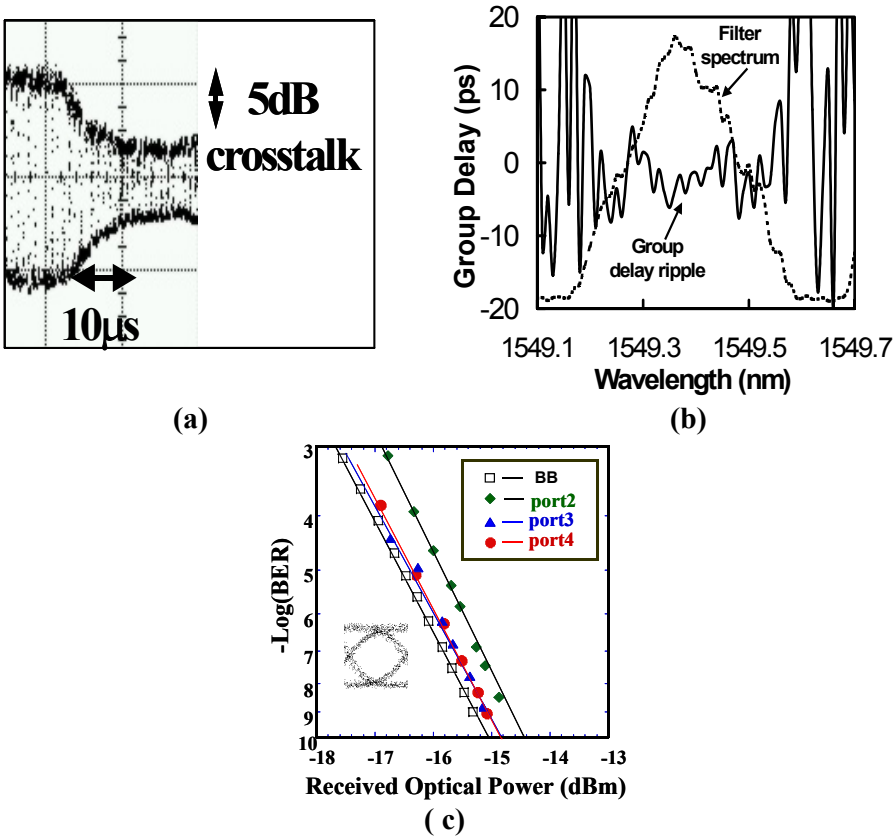

Figure 3.4.2 (a) Switching between ports 2 and 3. Switching time is 10 µs (b) Group delay ripple across the passband of a GTI filter port. The peak-to-peak ripple within the passband remains below ~5 ps (measured using modulation phase shift method with f_{mod} = 1 GHz and λ_{step}= 0.01nm) (c) BER measurement of 10 Gb/s modulated 1548 nm signal through each of the ports

3.4.2 Rapid code hopping in a time-wavelength two-dimensional OCDMA system

Optical code-division multiple access (OCDMA) has emerged as an attractive means for providing secure, asynchronous digital communication between multiple users [23]. One approach for alleviating the need for small chip time in traditional OCDMA has been the introduction of two-dimensional (2-D) OCDMA architecture, in which each bit is sub-divided into a combination of chip

times and a discrete set of wavelengths [28]. Figure 3.4.1b shows how an OCDMA bit would be coded both in time and wavelength domains. Since wavelength-cyclic shifts of asynchronous orthogonal codes are usually orthogonal codes themselves, this (cyclic wavelength-tuning) property of GTI in company with the fast tuning speed of MEMS actuators make MEMS-tunable GTI a very good choice for enabling codehopping in flexible OCDMA systems.

3.5.3 Experimental setup

Figure 3.4.3 shows the experimental setup for demonstrating code hopping. Each data bit is coded into a combination of 3 wavelengths (1543.2 nm, 1548 nm, 1552.8 nm) and 8 chip times (one chip time interval is 100ps.). The 10Gbits/s pattern generator is programmed to have a 100 ps pulse during one bit period of

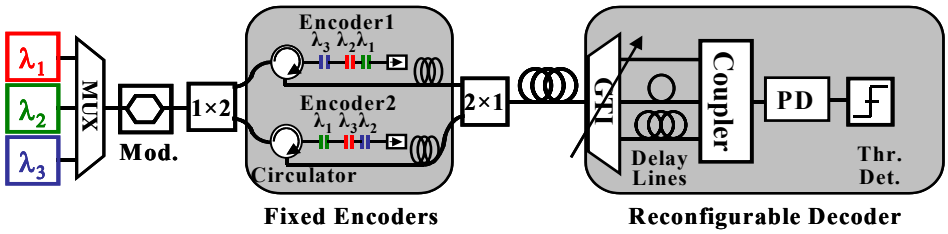

Figure 3.4.3 Experimental setup using the GTI as a tunable decoder in a time-wavelength OCDMA system. Transmission rate was 1.25 Gbits/s and each chip was 10 Gbits/s

800 ps if the data is "1" and no pulse if the data is "0". The Fiber Bragg Grating Arrays (FBGA) are used as fixed encoders that delay each wavelength according to the code. Coded data then passes through varying lengths of fiber (~20 m) to decorrelate the data for different users.

The encoded data from two users with cyclic codes are combined together and sent through the tunable GTI decoder. Different fiber lengths connected to the output ports of the GTI are used to realign the wavelengths of user and generate a peak pulse of level 3. The receiver output is fed into a threshold detector to

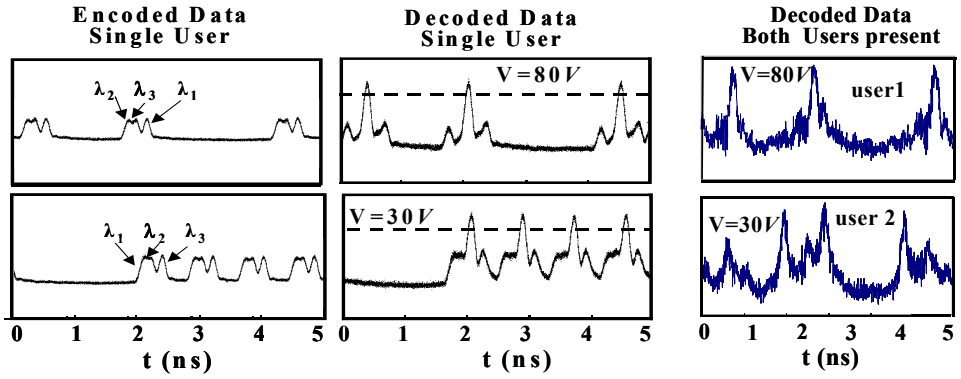

(a) (b) ©

Figure 3.4.4 By tuning the voltage of the GTI to 30V, user 1 is decoded and by applying voltage 80V, the second user is decoded. Figures (a) and (b) show the decoding when only one user is present. Figure (c) shows the code hopping when both users are present

recover the 1.25 Gb/s data. Figures 3.4.4a and b show that by just tuning the voltage of the GTI and without changing the delay lines, both codes for user 1 and 2 can be decoded. Figure 3.4.4c shows the decoding in the presence of both users. When one user is decoded, the other user will act as noise for the previous user. The crosstalk from GTI also behaves similar to Multiple Access Interference (MAI).

BIBLIOGRAPHY

1 G. P. Agrawal, "Nonlinear Fiber Optics", 2nd Edition

2 S. Chi and M.S.Kao, "*Bidirectional optical fiber transmission systems using Raman amplification*", J. of Lightwave Tech., **6**, 312-317, (1988).

3 A. R. Chraplyvy, "*Limitations on lightwave communications imposed by optical-fiber nonlinearities*," J. of Lightwave Technol., **8**, 1548-1557 (1990).

4 C. Dragone, et. al.*IEEE Photon. Technol. Let*t., vol. 3, pp. 812–815, Sept. 1991.

5 Ebrahimi, P.; Hauer, M.C.; Yu, Q.; Khosravani, R.; Gurkan, D.; Kim, D.W.; Lee, D.W.; Willner, A.E.*; "Statistics of polarization dependant gain in Raman fiber amplifiers due to PMD",* Lasers and Electro-Optics, 2001. CLEO '01.

6 Ebrahimi, P.; Wang, Y.; Sahin, A.B.; Yan, L.-S.; Willner, A.E.; Qian, Y.; Li, J.; ***"****Effects of SBS and Rayleigh scattering in densely-spaced bidirectional transmission using Raman amplification",* Lasers and Electro-Optics, 2002. CLEO '0

7 N. Gisin, R. Passy, J. C. Bishoff, and B. Perny, *IEEE Photonics Tech. Letters,* vol. 5, No. 7, pp. 819-821, July 1993.

8 P.J. Legg et. al.., IEEE Photonics Tachnology Letters, pp. 661-663, Vol.6, No.5, May 94

9 S. K. Liaw, K. P. Ho, C. Lin and S. Chi, "*Multichannel bidirectional transmission using a WDM MUX/DMUX pair and unidirectional in-line amplifiers*", IEEE Photon. Tech. Lett.. **9**, 1664 – 1997 (1997).

10 Lima, I.R., Jr.; Khosravani, R.; Ebrahimi, P.; Ibragimov, E.; Willner, A.E.; Menyuk, *C.R.;* "Polarization mode dispersion emulator" Optical Fiber Communication Conference, 2000

11 D. Mahgerefteh, H.Y. Yu, D. L. Butler, J. Goldhar, D. Wang, E. Golovchenko, A. N. Pilipetskii, C. R. Menyuk and L. J. Joneckis, "*Effect of randomly varying birefringence on the Raman gain in optical fibers,*" CLEO '97, CThW5 (1997)

12 D. Marcuse, C.R. Menyuk, and P.K.A. Wai, *Journal of Lightwave Technology*, Vol. 15, No. 9, pp. 1735-46, Sep. 97.

13 S. Min, Y. Won;" Upper-bounds on bit error rate of OCDMA systems using the time spreading/ wavelength hopping codes"**,** Lasers and Electro-Optics Society 2000 Annual Meeting.

14 O. Moreno, et. al., IEEE Trans. On Information Theory, vol. 41, no. 2, 1995

15 Y.Namihira, T. Kawazawa, and H. Wakabayashi, Electronics Lett., vol. 29, p. 32, 1993.

16 M. Nissov, K. Rottwitt, H.D. Kidorf and M.X. Ma, "*Rayleigh crosstalk in long cascades of distributed unsaturated Raman amplifiers*", Electronics Letters, **35**, 997 - 998 (1999).

17 Ohtsuki, T.; "Performance analysis of direct-detection optical asynchronous CDMA systems with double optical hard-limiters" IEEE International Conference on Communications, 1997.

18 R. Paschotta, G. J. Spühler, D.H. Sutter, N. Matuschek, U. Keller, M. Moser, R. Hövel, V. Scheuer, G. Angelow and T. Tschudi, "Double-chirped semiconductor mirror for dispersion compensation in femtosecond lasers", Appl. Phys. Lett., vol. 75, No. 15, pp. 2166-2168, 1999.

19 C. D. Poole, R.E. Wagner, Electronics Letters, vol.22, No.19, pp. 1029-30, Sep. 1986.

20 C.D. Poole, Opt. Lett., 13, 687-689, 1988.

21 C. H. Prola, Jr., J. A. Pereira da Silva, A. O. Dal Forno, R. Passy, J. P. von der Weid, and N. Gisin, *IEEE Photonics Tech. Letters*, vol. 9, No. 6, pp. 842-844, June 1997.

22 J. Sakai, and T. Kimura, IEEE J. Quantum Electronics, QE-17, 1041-1051, 1981.

23 J. A. Salehi, C.A. Brackett, "Code division multiple-access techniques in optical fiber networks. Parts I and II." IEEE Transactions on Communications, Vol. 37, no. 8,1989.

24 A. Stok, E. H. Sargent, "Lighting the local area: Optical code-division multiple access and quality of service provisioning," IEEE Network, Nov/Dec 2000.

25 R.H. Stolen,*"Polarization effects in fiber Raman and Brillouin lasers,"* IEEE J. Quantum Electronics, QE-15, 1157 (1979)

26 H. Suzuki, N. Takachio, H. Masuda and M. Koga, "*50GHz spaced, 32 X 10 Gbit/s dense WDM transmission in zero-dispersion region over 640km*

of dispersion-shifted fibre with multiwavelength distributed Raman amplification," Electronics Letters, Vol. 35, No. 14, pp. 1175-1176 (1999)

27 N. Tacachio and H. Suzuki, "*Application of Raman-distributed amplification to WDM transmission systems using 1.55-□m dispersion-shifted fiber*", J. of Lightwave Technology, **19**, 60-69, (2001).

28 L. Tancevski, I. Andonovic, "Hybrid wavelength hopping/time spreading code division multiple access systems," IEE Proc. Optoelectron., vol. 143, no. 3, June 1996.

29 M. O. Van Deventer, J. J. G. M van der Tol and A. J. Boot, "*Power penalties due to Brillouin and Rayleigh scattering in a bidirectional coherent transmission system*," IEEE Photon. Tech. Lett.. **6**, 291-294 (1994).

30 G.-C. Yang, W. C. Kwong, "Performance comparison of multiwavelength CDMA and WDMA + CDMA for fiber-optic networks," IEEE Trans. Commun., vol. 45, no. 11, Nov. 1997.

31 G.-C. Yang, W. C. Kwong, "Performance comparison of multiwavelength CDMA and WDMA + CDMA for fiber-optic networks," IEEE Trans. Commun., vol. 45, no. 11, Nov. 1997.

32 K. Yu, et. al., Lasers and Electro-Optics Society 2003 Annual Meeting, LEOS'03, Paper WE4, Oct., 2003

33 .J. Zhang, V. Dominic, M. Misey, S. Sanders, and D. Mehuys, "*Dependence of Raman Polarization Dependent Gain on Pump Degree of Polarization at High Gain Levels*," OAA '00, OMB4 (2000)